Hindawi Publishing Corporation
Journal of Nanomaterials
Volume 2015, Article ID 562938, 12 pages
http://dx.doi.org/10.1155/2015/562938

Research Article

Dioscorea bulbifera Mediated Synthesis of Novel $Au_{core}Ag_{shell}$ Nanoparticles with Potent Antibiofilm and Antileishmanial Activity

Sougata Ghosh,[1] Soham Jagtap,[1] Piyush More,[1] Usha J. Shete,[2] Neeraj O. Maheshwari,[2] Shilpa J. Rao,[3] Rohini Kitture,[4] Sangeeta Kale,[4] Jayesh Bellare,[5] Shivprasad Patil,[2] Jayanta K. Pal,[3] and Balu A. Chopade[6]

[1]*Institute of Bioinformatics and Biotechnology, University of Pune, Pune 411007, India*
[2]*Nanomechanics Laboratory, Department of Physics, Indian Institute of Science Education and Research, Pune 411008, India*
[3]*Cell and Molecular Biology Laboratory, Department of Biotechnology, University of Pune, Pune 411007, India*
[4]*Department of Applied Physics, Defense Institute of Advanced Technology, Girinagar, Pune 411025, India*
[5]*Department of Chemical Engineering, Indian Institute of Technology, Bombay, Powai, Mumbai 400076, India*
[6]*Department of Microbiology, University of Pune, Pune 411007, India*

Correspondence should be addressed to Balu A. Chopade; chopade@unipune.ac.in

Received 2 December 2014; Revised 12 March 2015; Accepted 19 March 2015

Academic Editor: Sherine Obare

Copyright © 2015 Sougata Ghosh et al. This is an open access article distributed under the Creative Commons Attribution License, which permits unrestricted use, distribution, and reproduction in any medium, provided the original work is properly cited.

Dioscorea bulbifera is a potent medicinal plant used in both Indian and Chinese traditional medicine owing to its rich phytochemical diversity. Herein, we report the rapid synthesis of novel $Au_{core}Ag_{shell}$ nanoparticles by *D. bulbifera* tuber extract (DBTE). $Au_{core}Ag_{shell}$ NPs synthesis was completed within 5 h showing a prominent peak at 540 nm. HRTEM analysis revealed 9 nm inner core of elemental gold covered by a silver shell giving a total particle diameter upto 15 nm. $Au_{core}Ag_{shell}$NPs were comprised of 57.34±1.01% gold and 42.66 ± 0.97% silver of the total mass. $Au_{core}Ag_{shell}$NPs showed highest biofilm inhibition upto 83.68 ± 0.09% against *A. baumannii*. Biofilms of *P. aeruginosa*, *E. coli*, and *S. aureus* were inhibited up to 18.93 ± 1.94%, 22.33 ± 0.56%, and 30.70 ± 1.33%, respectively. Scanning electron microscopy (SEM) and atomic force microscopy (AFM) confirmed unregulated cellular efflux through pore formation leading to cell death. Potent antileishmanial activity of $Au_{core}Ag_{shell}$NPs (MIC = 32 μg/mL) was confirmed by MTT assay. Further SEM micrographs showed pronounced deformity in the spindle shaped cellular morphology changing to spherical. This is the first report of synthesis, characterization, antibiofilm, and antileishmanial activity of $Au_{core}Ag_{shell}$NPs synthesized by *D. bulbifera*.

1. Introduction

Recent advances in the field of nanotechnology encompass the development of safe and ecofriendly route towards the synthesis of nanoparticles for the benefit of human health. Gold nanoparticles (AuNPs) with unique physicochemical and optical properties are reported to have potent applications in photonics, chemical sensing as well as biomedical applications like photothermal therapy and drug delivery [1–4]. Silver nanoparticles (AgNPs) are considered to be superior to other nanostructured inorganic metal particles due to their well-known electrical conductivity, optical properties, and oxidative catalysis [5, 6]. AgNPs are used in different fields in medicine due to their broad spectrum antimicrobial effect [7–10]. Therefore, AgNPs have found their applications in various pharmaceutical products, such as water purification systems, burn dressings, and medical devices [11, 12]. Thus, combination of both gold and silver to synthesize bimetallic $Au_{core}Ag_{shell}$NPs is of utmost scientific rationale. However, till date there are no well-defined biological routes for synthesizing $Au_{core}Ag_{shell}$NPs with therapeutic potential.

Among various medicinal plants used in Ayurveda, Indian system of traditional medicine, *Dioscorea bulbifera* is noteworthy owing to its multiple therapeutic

potential [13, 14]. It is reported to exhibit antimicrobial, plasmid curing, analgesic, anti-inflammatory, antihyperglycemic, antihyperlipidemic, antinociceptive, and antitumor activities [15–19]. Recently, we have reported its antidiabetic and antioxidant potential [20–22]. Additionally, we have reported the potential of *D. bulbifera* in synthesizing both AgNPs and AuNPs owing to its rich phytochemistry containing both reducing agents and stabilizing agents [7, 23]. However, there are no reports up to date on synthesis of bimetallic nanoparticles using *D. bulbifera*.

Multidrug resistant (MDR) Gram negative and Gram positive bacteria like *Acinetobacter baumannii* and *Staphylococcus aureus*,respectively, have emerged as highly infectious nosocomial pathogens owing to their remarkable resistance to antibiotics, metal salts, desiccation, and disinfectants [24–28]. Such type of pathogenesis among the critically ill and immune-compromised patients is characterized by the biofilm formation that comprise of a complex, organized bacterial community adhering to the surface forming microcolonies composed of exopolymeric matrix of carbohydrates, proteins, and nucleic acids [29–32]. Hereby, the bacteria gain ability to evade the host defenses, resistance to antibiotic therapy and deliberate delocalization of planktonic bacteria resulting in implantation, and colonization at newer sites, causing nascent acute infections in the host [33]. Currently, there are no reports on the application of bimetallic nanoparticles composed of gold and silver, in controlling the biofilm formation which can prove to be a powerful therapeutic strategy.

In view of the above background, we report for the first time the synthesis of $Au_{core}Ag_{shell}$NPs by *D. bulbifera* tuber extract (DBTE) followed by characterization using UV-visible spectroscopy, high resolution transmission electron microscopy (HRTEM), energy dispersive spectroscopy (EDS), and dynamic light scattering (DLS). Bioreduced $Au_{core}Ag_{shell}$NPs were checked for the biofilm inhibitory activity against *A. baumannii*, *P. aeruginosa*, *E. coli*, and *S. aureus* employing field emission scanning electron microscopy (FESEM) and atomic force microscopy (AFM).

2. Materials and Methods

2.1. Synthesis of Gold Core Silver Shell Nanoparticles ($Au_{core}Ag_{shell}$NPs). DBTE was prepared as per our earlier report [7]. In brief, fresh tubers of *D. bulbifera* were washed thoroughly and chopped into slices and shade dried followed by grinding into fine powder. 5 g of the powder was boiled in 100 mL of distilled water for 5 min and decanted followed by filtration. Synthesis was initiated by addition of 5 mL of DBTE to 95 mL of aqueous solution with 1 mM $HAuCl_4$ and 0.7 mM of $AgNO_3$ followed by incubation at 50°C for 5 h. The progress of reduction was monitored by measuring the UV-visible spectra of the solution at regular intervals on a spectrophotometer (SpectraMax M5, Molecular Devices Corp, USA) operated at resolution of 1 nm. Bioreduced $Au_{core}Ag_{shell}$NPs synthesized by DBTE were centrifuged at 10,000 rpm for 15 min at room temperature, followed by redispersal of the pellet in sterile distilled water to remove any uncoordinated biological molecules. Repetition of alternate centrifugation and redispersion in sterile distilled water for three times ensured better separation of free entities from the nanoparticles which were used for all further biological activities.

2.2. Transmission Electron Microscopy (TEM), High Resolution Transmission Electron Microscopy (HRTEM), and Dynamic Light Scattering (DLS) Measurements. Shape and size of the bioreduced $Au_{core}Ag_{shell}$NPs were determined using TEM (Tecnai 12 cryo TEM, FEI, Netherland) and was confirmed by JEOL-JEM-2100 higher resolution transmission electron microscope (HRTEM) coupled with elemental composition mapping under scanning transmission electron microscopic mode (STEM). Energy dispersive spectra of $Au_{core}Ag_{shell}$NPs, recorded in the energy dispersive spectrometer (EDS) equipped in JEOL JSM 6360A analytical scanning electron microscope at an energy range 0–20 keV confirmed the synthesis of $Au_{core}Ag_{shell}$NPs. Particle size was analyzed using the dynamic light scattering equipment (Zetasizer Nano-2590, Malvern Instruments Ltd, Worcestershire, UK) in polystyrene cuvette.

2.3. Antibiofilm Activity. 5 μL, OD_{600} (0.05) adjusted overnight grown cultures of *A. baumannii*, *P. aeruginosa*, *E. coli*, and *S. aureus* were incubated in absence and in presence of $Au_{core}Ag_{shell}$NPs at various concentrations ranging from 1 to 1024 μg/well in Mueller Hinton broth in 96 well microtitre plates. Negative controls (no cells) were included for each of the experimental preparations. The microtitre plates were then incubated overnight at 37°C under static conditions and processed thereafter. Nonadherent cells were removed from microtitre by aspiration. Wells containing biofilm matrices were washed thrice with sterile PBS followed by staining with 0.1% gentian violet (HiMedia, India) for 10 min at room temperature. Excess stain was removed by immersing in water trough followed by drying in laminar air flow. Finally, 200 μL of absolute ethanol was added to each well and shaken at 1020 rpm for 10 sec. Absorbance at 570 nm was recorded in a multiplate reader. Biofilm indices were calculated after normalizing with appropriate controls. All biofilm assays were repeated thrice.

2.4. Visualization of Biofilm Employing SEM and AFM. The biofilm inhibition was carried out on sterile grease free glass cover slips as per the above mentioned procedure with a final volume of 2 mL in 6 well plates. After 24 h, cover slips were washed with sterile PBS followed by fixation with glutaraldehyde which was further dehydrated sequentially using ethyl alcohol and analyzed using scanning electron microscope (SEM, JEOL JSM 6360A).

2.5. Atomic Force Microscopy. Imaging of the cell surface was performed using JPK Nano-wizard II (Germany) AFM setup in intermittent contact (IC) mode in air. Images were recorded in height and deflection (amplitude) modes where deflection mode gives higher contrast in morphological details and height image provide sample surface topography. Silicon nitride tips were used with the tip radius < 10 nm, spring constant of 40 N/m and resonant frequency

of 300 KHz for IC mode [34]. Line rate of 0.5–1 Hz was used for topographical (height) and deflection images. Elastic properties like Young's Modulus of the treated and untreated biofilm samples were evaluated where the cantilever served as soft nanoindenter allowing local testing of small and inhomogeneous samples. Hertzian model of contact theory for indentation with spherical tips was used to evaluate Young's Modulus [35–39]. The cantilever was modified by gluing (Dymax-OPV 30 UV curable glue) 20 μM glass bead to the tip. The spring constant of the cantilever was determined using thermal noise analysis in liquid while glass was used as rigid surface to calibrate the photo detector sensitivity. Force curves were recorded at the rate of 5 μM/sec with typical piezodisplacement of 1 μM–10 μM. Ensemble of 64 force curves was obtained on different locations of the cell surfaces. Analysis of the force curves was done using JPK data processing software. The mean values of Young's modulus were calculated as the average, weighted over the data obtained by analysis of 64 curves from each independent experiment. Young's modulus is calculated by the equation [36, 38, 40]

$$F = \frac{4ER^{0.5}\delta^{1.5}}{3\left(1-\nu^2\right)}, \qquad a = (R\delta)^{1/2}, \tag{1}$$

where F is the force applied by the cantilever, E is Young's Modulus, δ is the indentation depth, R is the radius of the bead (10 um), a is the contact radius, and ν is Poisson's ratio (0.5 for biological samples).

2.6. Antileishmanial Activity. Promastigotes of *Leishmania donovani* (MHOM/IN/83/Ag83) were cultured in Medium 199 (Sigma, St. Louis, MO) supplemented with 10% heat inactivated foetal bovine serum (FBS) (Sigma, St. Louis, MO) at 25°C. The parasites were maintained *in vitro* by subpassaging them every fifth day. Antileishmanial activity of $Au_{core}Ag_{shell}$NPs was investigated using MTT (3-(4,5-dimethyl-thiazol-2-yl)-2,5-diphenyl-tetrazolium bromide) assay. Logarithmic phase *L. donovani* promastigotes (2×10^5 parasites/mL) were seeded in a 96-well microtitre plate and treated with the nanoparticles followed by incubation at 25°C for 72 h.

2.7. SEM and AFM Analysis. 72 h treated *L. donovani* promastigotes were adhered to poly-L-lysine coated cover slips and fixed with 4% paraformaldehyde for 15 min at room temperature which were subjected to SEM and AFM analysis as per the procedure described in the earlier section.

2.8. DNA Fragmentation Assay. The assay was carried as described in earlier report by Herrmann et al., 1994 with a slight modification [41]. Briefly, *L. donovani* promastigotes were treated with nanoparticles for 72 h. The pellets were treated with lysis buffer (1% NP-40 in 2 mM EDTA, 50 mM Tris-HCl, pH 7.5) followed by centrifugation at 1600 ×g for 5 min. The supernatant was brought to 1% SDS and treated with RNAase (5 μg/μL) for 2 h at 56°C. Proteinase K (2.5 μg/μL) treatment was given for 3 h at 37°C followed by precipitation of DNA with 1/2 volume 10 M ammonium acetate and 2.5 volume ethanol. The DNA was dissolved in TE buffer (Tris 10 mM, EDTA 1 mM, pH 8.0) and analyzed by agarose gel electrophoresis.

3. Results

3.1. UV-Visible Spectroscopy. DBTE mediated reduction of silver and gold ions in aqueous solution was confirmed by the gradual change in color from orange red to dark reddish violet as a function of reaction time. UV-vis spectra recorded from 0 to 5 h revealed a distinct and clear increase in intensity of the gold surface plasmon band, while a well-defined band corresponding to AgNPs was not observed in case of $Au_{core}Ag_{shell}$NPs (Figure 1(a)). Although no significant synthesis was observed from 0 to 0.5 h, but thereafter the rate of reduction took a rapid pace, almost completing the reduction within 4 h, with a slight increase in the intensity till 5 h. UV-vis spectra confirmed the synthesis of $Au_{core}Ag_{shell}$NPs which showed a peak at 540 nm unlike that of individual AgNPs at 440 nm (Figure 1(b)). However, a decrease in the peak intensity was observed in case $Au_{core}Ag_{shell}$NPs as compared to that of individual AuNPs at 540 nm which might be attributed due to formation of the silver shell onto a gold core.

3.2. TEM, HRTEM, and EDS Analysis. TEM images confirmed the size, shape, and nature of bioreduced nanoparticles. TEM images distinguished the shell from the core with prominent boundary between the two layers (Figure 2(a)). The diameter of the inner core was in a range between 5 and 11 nm while the entire particle showed a diameter of 13 to 19 nm. Particles were found to be almost monodispersed, the majority being spherical with a core represented by dark contrast surrounded by a shell with a lighter shade. Aggregation was not observed indicating the stable nature of the particles. HRTEM analysis was also in agreement with the TEM analysis where the diameter of the core and the entire particle was measured to be 6 to 10 nm and 13 to 18 nm, respectively (Figure 2(c)). Lattice fringes were clearly observed on the surface of the nanoparticles confirming the crystalline nature (Figure 2(c)). Additionally, elemental mapping clearly indicated the location of elemental silver and gold in the core shell nanoparticles (Figure 2(d)). It was distinctly evident that gold formed the core while silver formed the shell of the nanoparticles confirming the fact that the bioreduced nanoparticles were $Au_{core}Ag_{shell}$ in nature. EDS results confirmed the presence of both elemental silver as well as elemental gold in the nanoparticles. $Au_{core}Ag_{shell}$NPs were comprised of 57.34 ± 1.01% gold and 42.66 ± 0.97% silver of the total mass (Figure 2(b)). Particle size analysis exhibited a variation mostly between 7 and 18 nm, the majority being 10 nm (Figure 2(a)).

3.3. Biofilm Inhibitory Activity. Biofilm inhibition studies revealed a high efficacy and selectivity of $Au_{core}Ag_{shell}$NPs towards controlling bacterial pathogens. $Au_{core}Ag_{shell}$NPs, at a concentration of 100 μg/mL, could inhibit biofilm formation

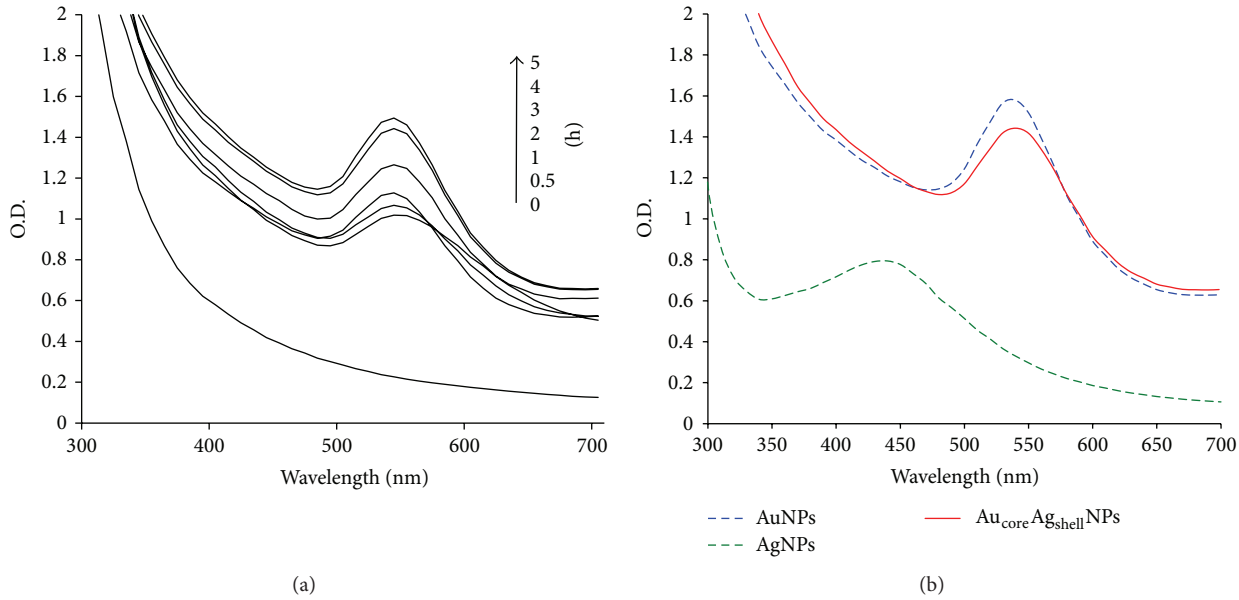

Figure 1: Ultraviolet-visible characterization. (a) UV-vis spectra recorded as a function of reaction time for synthesis of $Au_{core}Ag_{shell}$NPs by DBTE at 40°C. (b) Comparative ultraviolet-visible spectra recorded for AuNPs, AgNPs and $Au_{core}Ag_{shell}$NPs after complete bioreduction by DBTE for 5 h at 40°C.

up to 83.68 ± 0.09% against *A. baumannii* (Figure 3). However, $Au_{core}Ag_{shell}$NPs showed a comparatively lower activity equivalent to 18.93 ± 1.94% against *P. aeruginosa* at the same concentration. Biofilm formation in case of *E. coli* was inhibited up to 22.33 ± 0.56% which was found to be superior to *P. aeruginosa* while inferior as compared to *A. baumannii*. It is important to note that the biofilm formation was inhibited up to 30.70 ± 1.33% even against Gram positive bacteria like *S. aureus*.

3.4. Scanning Electron Microscopy for Biofilm Inhibition. Scanning electron micrographs revealed the effective inhibition of biofilm by $Au_{core}Ag_{shell}$NPs against *A. baumannii*. Untreated biofilm were represented by confluent lawns (Figure 4(a-i)) with intact cellular morphology. Treatment with $Au_{core}Ag_{shell}$NPs exhibited marked biofilm inhibition with discrete cells on the glass surface instead of lawns (Figure 4(a-ii)). The treated cells showed irregular morphology owing to cell damage by the $Au_{core}Ag_{shell}$NPs. A similar observation was achieved in case of *P. aeruginosa* as well. In case of the untreated cells a profound bacterial biofilm surrounded by exopolymeric slimy matrix was seen (Figure 4(b-i)). Treated cells exhibited biofilm inhibition characterized by prominent membrane disintegration leading to efflux of cellular materials (Figure 4(b-ii)). Size of *E. coli* cells were found to increase abruptly followed by efficient biofilm inhibition on treatment with $Au_{core}Ag_{shell}$NPs (Figure 4(c-ii)). Surface attachment was greatly compromised on treatment unlike the untreated cells which formed a compact biofilm due to effective adherence onto the glass surface (Figure 4(c-i)). In case of *S. aureus*, the untreated biofilm was characterized by groups of closely packed spherical cells (Figure 4(d-i)) which on treatment showed discontinuous biofilm consisting of sparsely packed cells in discrete aggregates. The cells in treated biofilm showed surface invaginations and deformities (Figure 4(d-ii)).

3.5. Atomic Force Microscopy. AFM images were recorded to confirm the effect of $Au_{core}Ag_{shell}$NPs treatment on bacterial biofilms which illustrated a packed lawn in case of untreated biofilms. The interrupted biofilms without packed morphology owing to compromised cell adhering capability in treated biofilm (Figure 5(a-ii)) were readily differentiated from the untreated bacterial biofilms (Figure 5(a-i)). *A. baumannii* showed complete elimination of biofilm characterized by discrete single cells attaching onto the glass surface. The measurements of elastic moduli showed that the treated cells (104.59 KPa) were stiffer as compared to untreated cells (0.82 KPa). *P. aeruginosa* biofilm exhibited cells embedded in the exopolymeric matrix while in case of treated biofilm, discrete cells were observed (Figures 5(b-i) and 5(b-ii)). Similar trend in the increase of stiffness in the treated cells (75.72 KPa) was observed compared to untreated cells (40.02 KPa). Untreated *E. coli* biofilm was characterized by evenly distributed uninterrupted confluent bacterial lawns while biofilms treated with $Au_{core}Ag_{shell}$NPs showed uneven cellular distribution with discrete solitary cells on the glass surface at large distances (Figures 5(c-i) and 5(c-ii)). Stiffness (57.64 KPa) in the treated biofilm increased as compared to untreated biofilm (22.84 KPa). Inhibition of *S. aureus* biofilms was clearly evident from the AFM micrographs showing the irregularly clumped cellular masses separated by large valleys unlike the untreated biofilm which exhibited profound uniform lawn (Figures 5(d-i) and 5(d-ii)). Stiffness in treated biofilm increased up to 197.45 KPa which was significantly higher compared to 48.63 KPa found for the untreated biofilm.

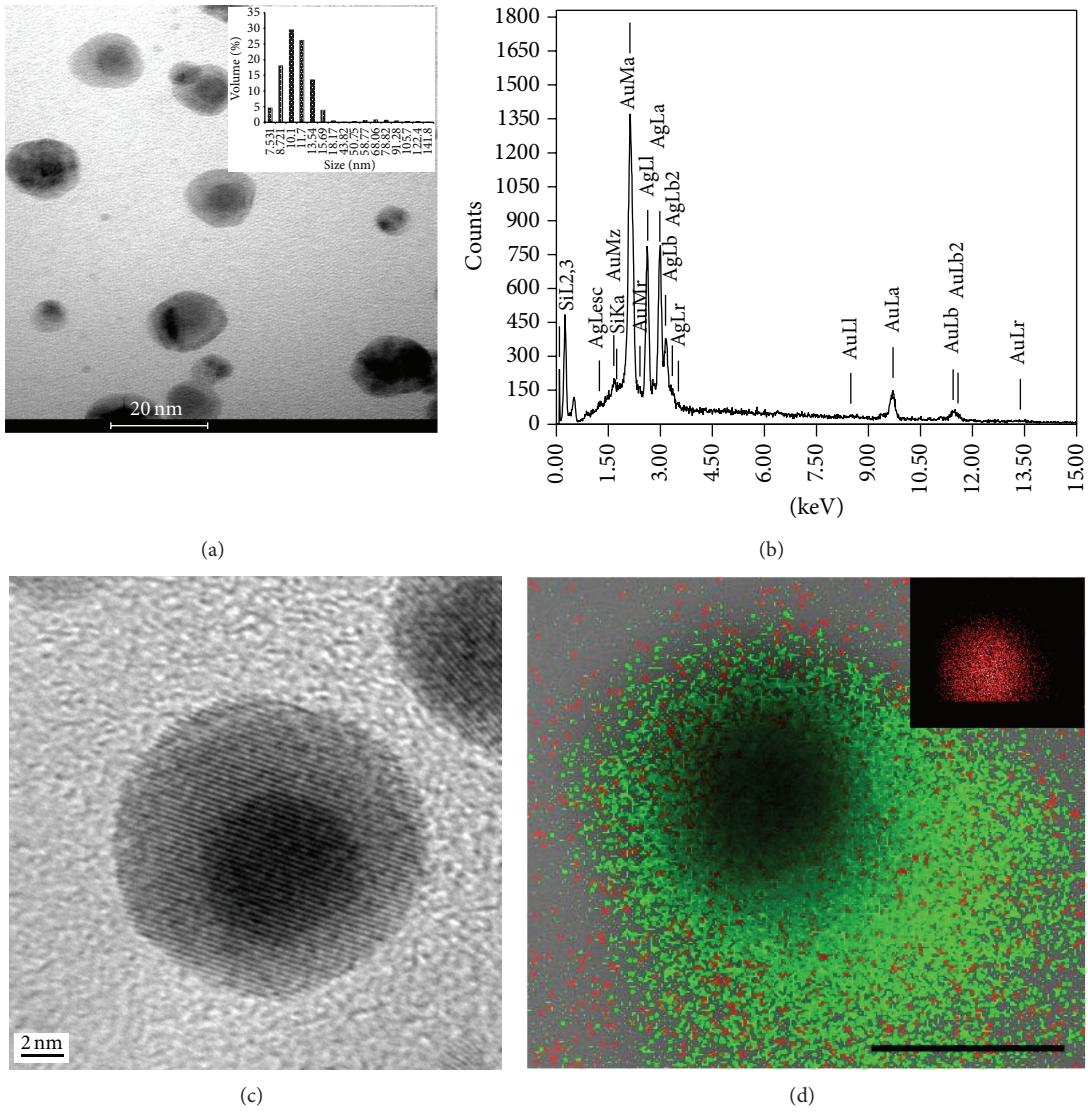

Figure 2: Micrographs of representative $Au_{core}Ag_{shell}$NPs synthesized by DBTE. (a) Transmission electron micrograph showing core shell nanoparticles. Inset represents the histogram for particle size distribution. (b) Representative spot EDS profile confirming the presence of both elemental Ag and Au in $Au_{core}Ag_{shell}$NPs synthesized by DBTE. (c) High resolution transmission electron micrographs of $Au_{core}Ag_{shell}$NPs with lattice fringes synthesized by DBTE. (d) Elemental mapping showing silver shell (green) and gold core (inset figure), with scale bar indicating 100 nm.

3.6. Antileishmanial Activity. The effect of $Au_{core}Ag_{shell}$NPs on *L. donovani* promastigotes was determined quantitatively by MTT. The parasites were killed effectively on treatment with $Au_{core}Ag_{shell}$NPs (MIC = 32 μg/mL). SEM micrographs of untreated cells showed intact spindle shaped morphology tapering at both ends with a long flagellum which is typical for *L. donovani* healthy promastigote (Figure 6(a)). However, cells treated with $Au_{core}Ag_{shell}$NPs showed a pronounced deformation characterized by complete loss of spindle shaped morphology finally becoming spherical (Figure 6(b)). Similar results were also obtained in case of AFM micrographs (Figures 6(c) and 6(d)) which confirmed the antileishmanial potential that were further supported by DNA fragmentation (Figure 6(e)).

4. Discussion

D. bulbifera is considered as most important medicinal plant in both Indian and Chinese traditional medicine due to its multidimensional therapeutic potential owing to diverse phytochemicals. In this study, we found a route for rapid and efficient synthesis of $Au_{core}Ag_{shell}$NPs by DBTE within 5 h. In our earlier report, AuNPs were found to be formed rapidly within 90 min using *D. bulbifera*; however, synthesis of AgNPs was found to be completed at 5 h [7, 23]. Thus, the rapidly synthesized AuNPs acts as nanocrystalline seeds on which slowly formed AgNPs are uniformly deposited forming a complete coat on 9 nm Au core. Our results are in close correlation with the recent report on 11 nm

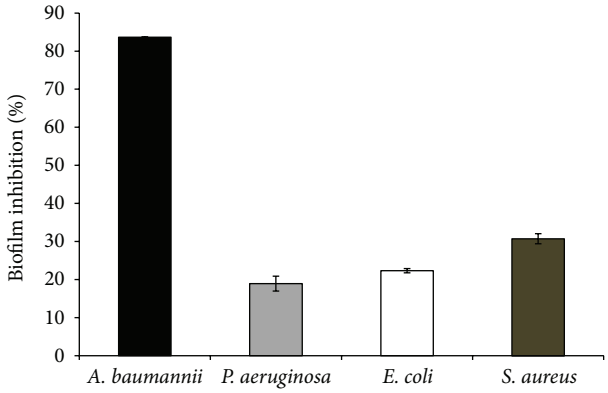

Figure 3: Inhibition of the growth of biofilm after treatment with $Au_{core}Ag_{shell}$NPs.

Au seed mediated chemical synthesis of 13 to 50 nm core shell nanoparticles using ascorbic acid as reductant and cetyltrimethylammonium chloride (CTAC) as capping agent [42]. Hereby, it is immensely important to note the promises of DBTE mediated rapid synthesis of exotic $Au_{core}Ag_{shell}$NPs as a novel route without involvement of any toxic chemicals. Phenolics and flavonoids might be the key players in the rapid synthesis while starch might stabilize the bioreduced nanoparticles which were composed of a gold core and a silver shell. Similarly citric acid and diosgenin may be responsible for the shape evolution. *D. bulbifera* tubers are reported to possess a rich phenolic and citric acid contents supporting the claim that fresh yam tubers are rich source of antioxidant that play a key role in prevention of oxidative stress mediated emergence of cancer and cardiovascular diseases [7, 43, 44]. Diosgenin and flavonoids and are also reported in *D. bulbifera* to promote antitumor and anticancer activity, respectively, which strongly support the potential of DBTE to synthesize $Au_{core}Ag_{shell}$NPs [19, 22, 45]. Synthesis of $Au_{core}Ag_{shell}$NPs was characterized by a peak at 540 nm which was similar to the report of Salunke et al. on synthesis of bimetallic nanoparticles (AgAuNPs) by *Plumbago zeylanica* indicating Au core and Ag shell [46]. DBTE synthesized $Au_{core}Ag_{shell}$NPs showed concentric spherical morphology strikingly different from both the polyhedral particles synthesized by polyol process and blunt ended nanopolygonal particles formed in preliminary reports on biological synthesis [46–48].

Bioreduced nanoparticles have found profuse utility in clinical studies and for designing novel therapeutic strategies. Adhesion and colonization lead to most emerging problem of biofilm associated microbial infections. Chronicity of nosocomial infections owing to enhanced persistence is a result of protective biofilms [49]. Hereby, DBTE synthesized $Au_{core}Ag_{shell}$NPs, exhibiting potent bacterial biofilm inhibition is a very significant finding towards development of new therapeutic strategy against microbial infections. This is the first report on antibiofilm activity of $Au_{core}Ag_{shell}$NPs, synthesized by DBTE against *A. baumannii* which was found to be considerably superior as compared to bimetallic nanoparticles synthesized by *P. zeylanica* [46]. Enhanced antibiofilm activity can be attributed by high surface to volume ratio [10, 50, 51]. Our results are concurrent with earlier reports which showed, in nanoparticulate form, metallic silver exhibits antibiofilm activity against *A. baumannii* at concentrations as high as 1024 μg/well [9, 46]. However, $Au_{core}Ag_{shell}$NPs inhibited the biofilm at a lower concentration of 100 μg/mL against *A. baumannii* which is one of the emerging most potent nosocomial multidrug-resistant pathogen. It poses threat due to its frequent outbreak causing urinary tract infection, meningitis, bacteremia, wound infections, and pneumonia. The ability of the pathogen to survive in diverse ecological niche and environmental conditions forming resistant biofilm facilitates its persistence on both inanimate and animate surfaces for extended periods of time [29, 52, 53]. Similarly it has been reported to gain resistance against multiple metal and metal ions as well in addition to antibiotics leading to compromised drug sensitivity [26–28, 54, 55]. Multidrug resistance associated bacteremia, osteomyelitis, and respiratory infections in patients suffering from traumatic injuries have high mortality rate in ICU, ranging from 26% to 68% [52, 56]. It is speculated that the mortality can be attributed to antimicrobial resistance, lower effectiveness of empirical therapy and scarcity of available therapeutic options. Hereby, the observed selectivity of the bioreduced $Au_{core}Ag_{shell}$NPs towards inhibition of *A. baumannii* biofilm is an immensely significant perspective which can be further exploited for designing powerful therapeutic strategy against *A. baumannii* infections.

$Au_{core}Ag_{shell}$NPs showed antibiofilm activity against *P. aeruginosa*, *E. coli* and *S. aureus* leading to damage of cell wall causing efflux of cellular materials. This may be attributed to the property of silver component to adhere to cell surface of bacteria, further generating reactive oxygen species leading to catalytic oxidation of cell membrane causing deformation and damage to the cell surface [7, 57]. Although, AgNPs are reported to inhibit the biofilms formed by *P. aeruginosa*, this is the first report on inhibition by spherical $Au_{core}Ag_{shell}$NPs synthesized by DBTE [58]. It is important to note that abrupt increase in bacterial cell length of *E. coli* was observed on treatment with $Au_{core}Ag_{shell}$NPs which is well in agreement with earlier report justifying gold to be responsible for the observed phenomenon [59]. $Au_{core}Ag_{shell}$NPs inhibited the biofilm formation in Gram positive *S. aureus* as well. Potential of the bioreduced nanoparticles might be attributed due to mechanisms like binding to cellular enzymes and proteins, specifically to SH-groups, interference with bacterial cell integrity and production and conservation of energy, as reported earlier against *Staphylococcus epidermidis* [8, 60–63]. DBTE synthesized $Au_{core}Ag_{shell}$NPs showed antileishmanial activity against *L. donovani* leading to complete disintegration of cellular morphology probably due to the silver component of the nanoparticles. Allahverdiyev et al. reported that AgNPs are leishmanicidal due to their capacity to produce ROS, owing to their large surface areas, smaller size, and ability to bind sulfur- and phosphor-containing groups [64].

5. Conclusion

This is the first report on synthesis of spherical $Au_{core}Ag_{shell}$NPs using DBTE which is a novel biological

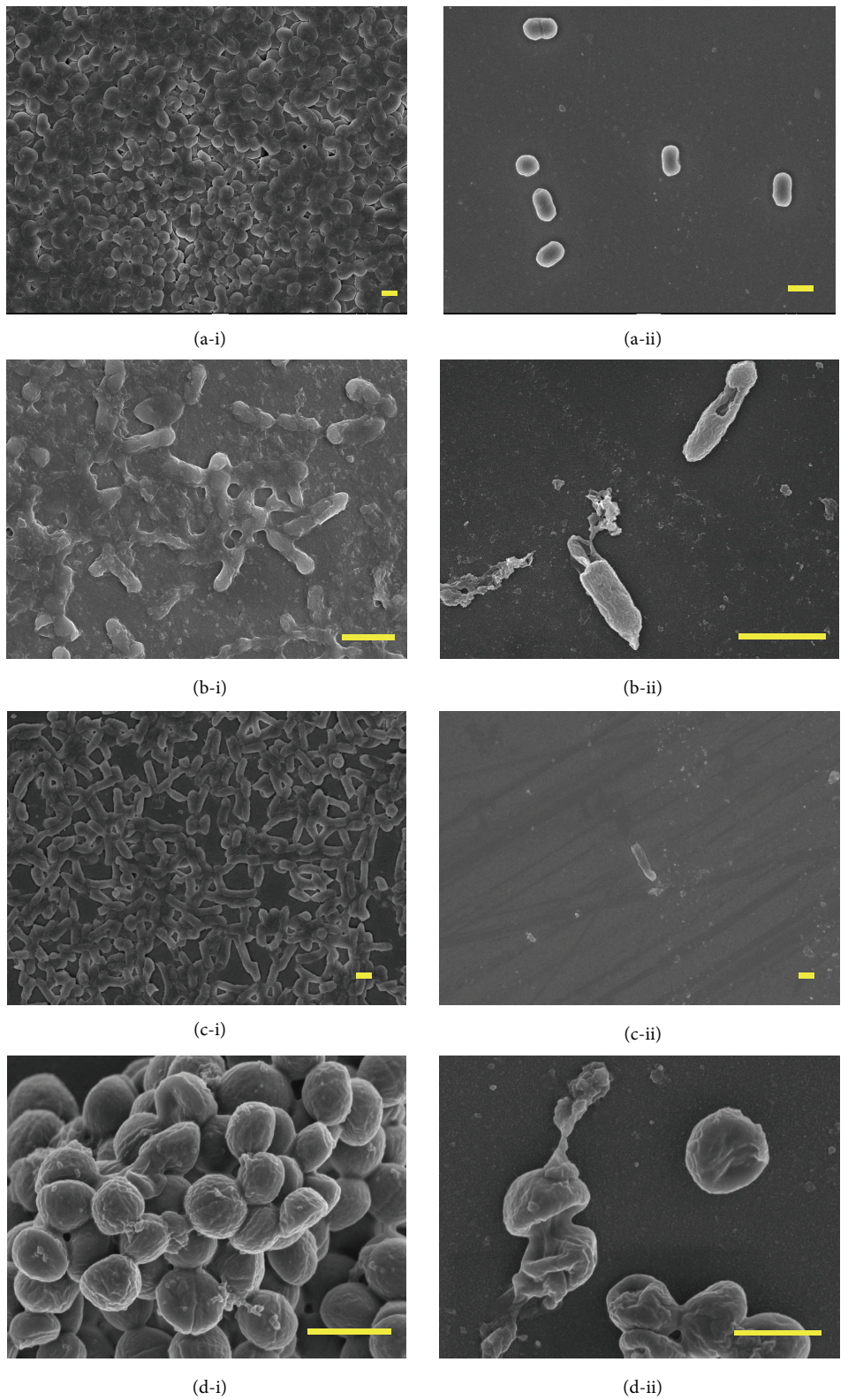

FIGURE 4: Scanning electron micrographs showing the architecture of untreated bacterial biofilm and biofilm treated with $Au_{core}Ag_{shell}$NPs. (a-i) Untreated biofilm of *A. baumannii* (inset scale bar representing 1 μm); (a-ii) *A. baumannii* biofilm treated with $Au_{core}Ag_{shell}$NPs (inset scale bar representing 1 μm); (b-i) untreated biofilm of *P. aeruginosa* (inset scale bar representing 1 μm); (b-ii) *P. aeruginosa* biofilm treated with $Au_{core}Ag_{shell}$NPs (inset scale bar representing 1 μm); (c-i) untreated biofilm of *E. coli* (inset scale bar representing 100 nm); (c-ii) *E. coli* biofilm treated with $Au_{core}Ag_{shell}$NPs (inset scale bar representing 1 μm); (d-i) untreated biofilm of *S. aureus* (inset scale bar representing 1 μm); (d-ii) *S. aureus* biofilm treated with $Au_{core}Ag_{shell}$NPs (inset scale bar representing 1 μm).

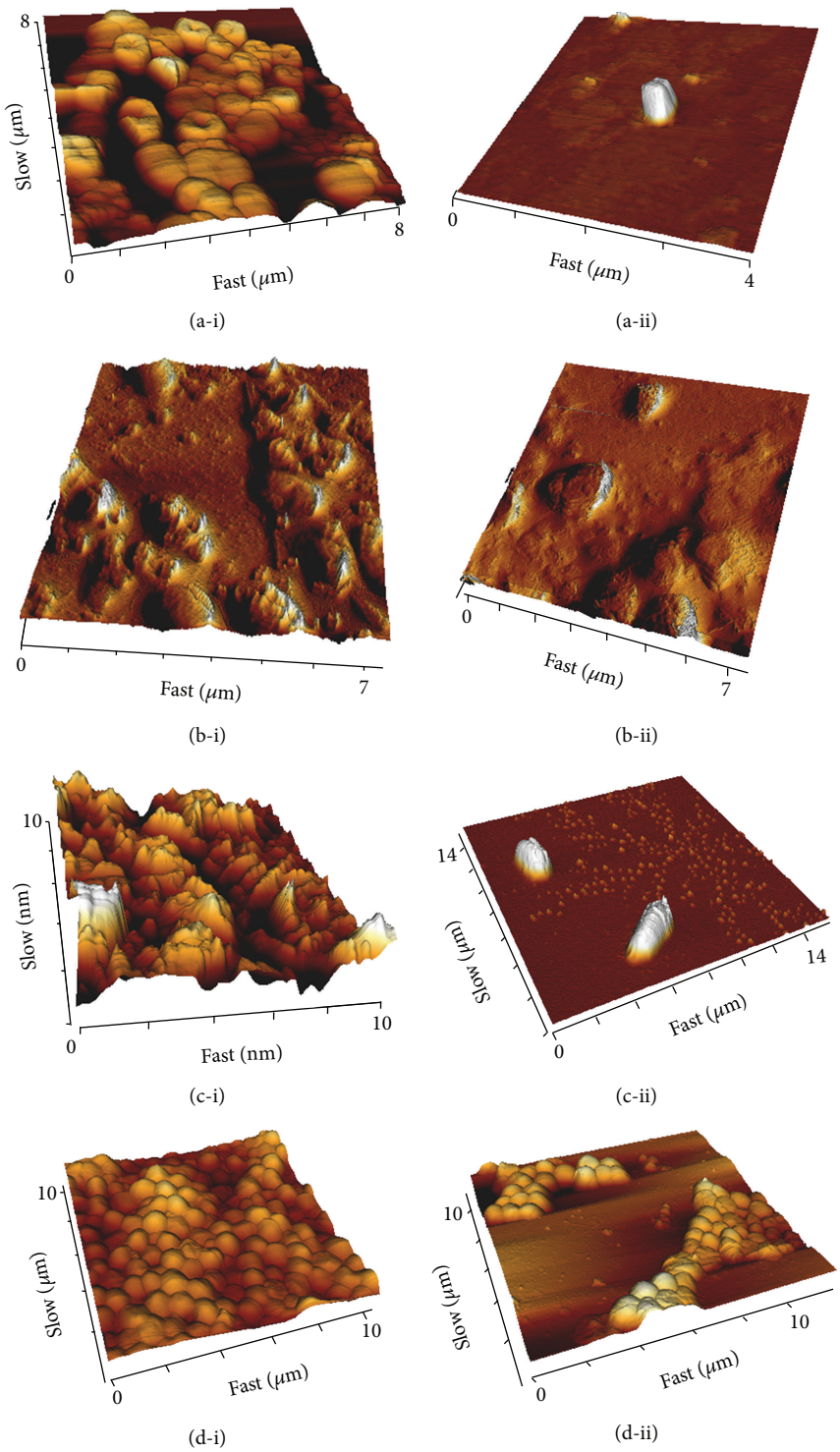

FIGURE 5: Representative three-dimensional (3D) atomic force micrographs of untreated bacterial biofilm and biofilm treated with $Au_{core}Ag_{shell}$NPs. (a-i) Untreated biofilm of *A. baumannii*; (a-ii) *A. baumannii* biofilm treated with $Au_{core}Ag_{shell}$NPs; (b-i) untreated biofilm of *P. aeruginosa*; (b-ii) *P. aeruginosa* biofilm treated with $Au_{core}Ag_{shell}$NPs; (c-i) untreated biofilm of *E. coli*; (c-ii) *E. coli* biofilm treated with $Au_{core}Ag_{shell}$NPs; (d-i) untreated biofilm of *S. aureus*; (d-ii) *S. aureus* biofilm treated with $Au_{core}Ag_{shell}$NPs.

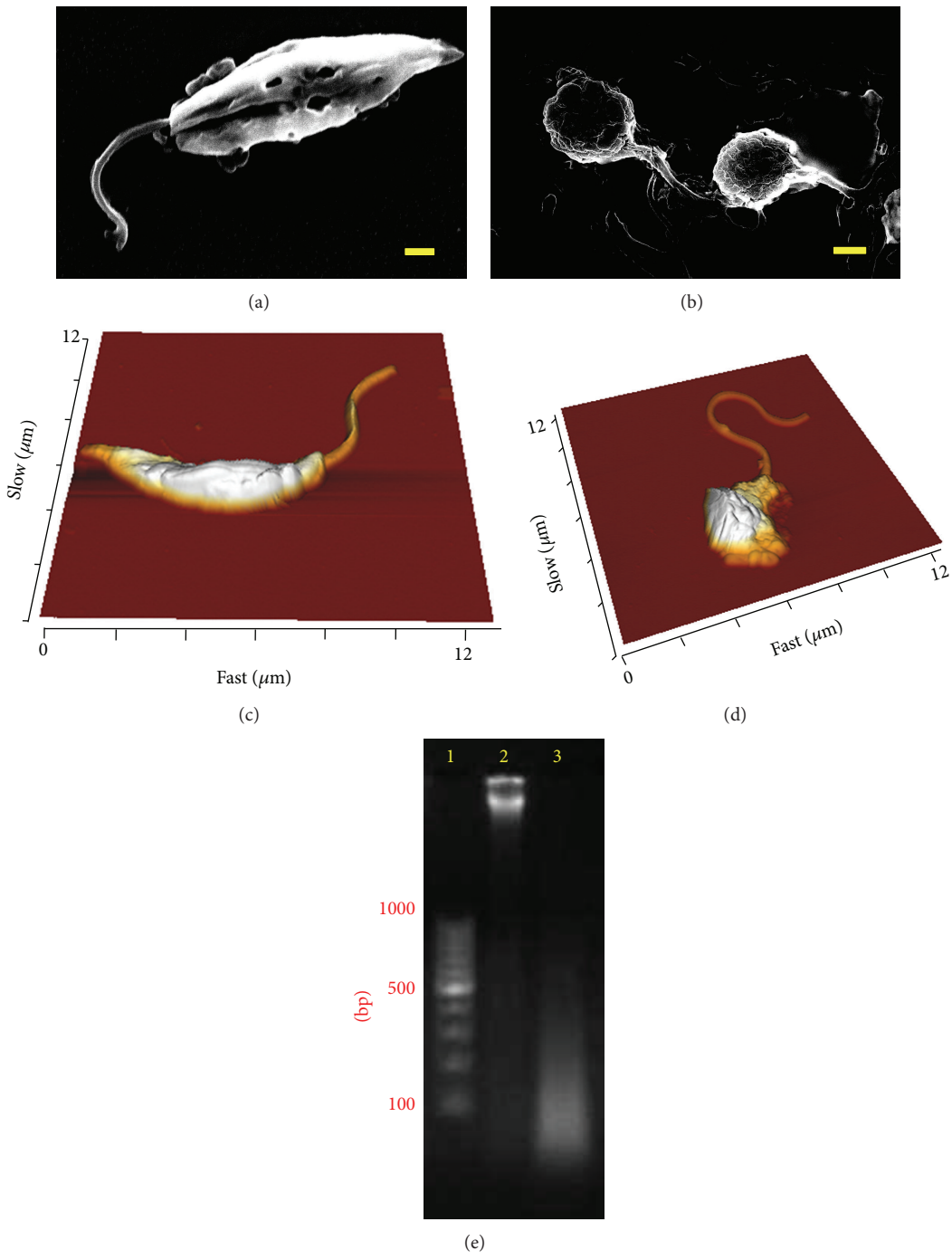

FIGURE 6: Morphological and molecular analysis for antileishmanial activity. (a) Representative scanning electron micrographs of untreated *L. donovani;* (b) SEM image of *L. donovani* after treatment with $Au_{core}Ag_{shell}$NPs (inset scale bar corresponds to 1 μm); (c) representative atomic force micrographs of untreated *L. donovani;* (d) AFM image of *L. donovani* after treatment with $Au_{core}Ag_{shell}$NPs; (e) induction of internucleosomal DNA fragmentation in *L. donovani* in response to treatment with $Au_{core}Ag_{shell}$NPs. Lane 1—100 bp ladder; Lane 2—untreated; Lane 3—$Au_{core}Ag_{shell}$NPs treated.

route for synthesis of nanoparticles with unique morphology with concentric Au core and Ag shell using medicinal plant, *D. bulbifera*. It showed efficient biofilm inhibition against Gram negative bacteria, particularly *A. baumannii* and Gram positive bacteria, *S. aureus*. The mechanism behind the biofilm inhibition was observed to be intense damage to the cells leading to disintegration of cell wall causing efflux of cellular materials. Similarly, it showed effective antileishmanial activity against *L. donovani*. Hence, the present study provides a strong scientific rationale for the use of DBTE synthesized $Au_{core}Ag_{shell}$NPs as potent antibiofilm and antileishmanial agent.

Conflict of Interests

The authors declare that there is no conflict of interests regarding the publication of this paper.

Acknowledgments

The authors acknowledge the use of TEM and HRTEM facilities in Chemical Engineering and CRNTS funded by the DST through Nanomission and IRPHA schemes. The authors thank Dr. M. Jayakannan, Indian Institute of Science Education and Research (IISER), Pune, for DLS facility. The authors also thank Mr. Sanjay Patil, Thematic Program Executive, Jawhar Unit, BAIF Development Research Foundation, Pune, India, for imparting knowledge about tribal usage and preparation of *D. bulbifera* as well as collection of plant samples. S. Ghosh thanks Council of Scientific and Industrial Research (CSIR, Government of India) for Senior Research Fellowship (09/137(0516)/2012-EMR-I). The authors acknowledge financial support for UPE Phase II for 2012–2017 by UGC, New Delhi, India.

References

[1] C. Peng, X. Duan, Z. Xie, and C. Liu, "Shape-controlled generation of gold nanoparticles assisted by dual-molecules: the development of hydrogen peroxide and oxidase-based biosensors," *Journal of Nanomaterials*, vol. 2014, Article ID 576082, 7 pages, 2014.

[2] S. Ghosh, S. Patil, M. Ahire et al., "*Gnidia glauca* flower extract mediated synthesis of gold nanoparticles and evaluation of its chemocatalytic potential," *Journal of Nanobiotechnology*, vol. 10, article 17, 2012.

[3] U. Shedbalkar, R. Singh, S. Wadhwani, S. Gaidhani, and B. A. Chopade, "Microbial synthesis of gold nanoparticles: current status and future prospects," *Advances in Colloid and Interface Science*, vol. 209, pp. 40–48, 2014.

[4] X. Huang, P. K. Jain, I. H. El-Sayed, and M. A. El-Sayed, "Gold nanoparticles: interesting optical properties and recent applications in cancer diagnostics and therapy," *Nanomedicine*, vol. 2, no. 5, pp. 681–693, 2007.

[5] Y. L. Balachandran, S. Girija, R. Selvakumar, S. Tongpim, A. C. Gutleb, and S. Suriyanarayanan, "Differently environment stable bio-silver nanoparticles: study on their optical enhancing and antibacterial properties," *PLoS ONE*, vol. 8, no. 10, Article ID e77043, 2013.

[6] Z. Zhang, L. Zhang, S. Wang, W. Chen, and Y. Lei, "A convenient route to polyacrylonitrile/silver nanoparticle composite by simultaneous polymerization-reduction approach," *Polymer*, vol. 42, no. 19, pp. 8315–8318, 2001.

[7] S. Ghosh, S. Patil, M. Ahire et al., "Synthesis of silver nanoparticles using *Dioscorea bulbifera* tuber extract and evaluation of its synergistic potential in combination with antimicrobial agents," *International Journal of Nanomedicine*, vol. 7, pp. 483–496, 2012.

[8] V. Alt, T. Bechert, P. Steinrücke et al., "An *in vitro* assessment of the antibacterial properties and cytotoxicity of nanoparticulate silver bone cement," *Biomaterials*, vol. 25, no. 18, pp. 4383–4391, 2004.

[9] S. Gaidhani, R. Singh, D. Singh et al., "Biofilm disruption activity of silver nanoparticles synthesized by *Acinetobacter calcoaceticus* PUCM 1005," *Materials Letters*, vol. 108, pp. 324–327, 2013.

[10] R. Singh, P. Wagh, S. Wadhwani et al., "Synthesis, optimization and characterization of silver nanoparticles from *Acinetoacter calcoaceticus* and their enhanced antibacterial activity when combined with antibiotics," *International Journal of Nanomedicine*, vol. 8, pp. 4277–4290, 2013.

[11] V. Thomas, M. M. Yallapu, B. Sreedhar, and S. K. Bajpai, "A versatile strategy to fabricate hydrogel-silver nanocomposites and investigation of their antimicrobial activity," *Journal of Colloid and Interface Science*, vol. 315, no. 1, pp. 389–395, 2007.

[12] S. Kim and H.-J. Kim, "Anti-bacterial performance of colloidal silver-treated laminate wood flooring," *International Biodeterioration & Biodegradation*, vol. 57, no. 3, pp. 155–162, 2006.

[13] R. N. Okigbo, C. L. Anuagasi, J. E. Amadi, and U. J. Ukpabi, "Potential inhibitory effects of some African tuberous plant extracts on *Escherichia coli, Staphylococcus aureus* and *Candida albicans*," *International Journal of Integrative Biology*, vol. 6, no. 2, pp. 91–98, 2009.

[14] R. B. Teponno, A. L. Tapondjou, D. Gatsing et al., "Bafoudiosbulbins A, and B, two anti-salmonellal clerodane diterpenoids from *Dioscorea bulbifera* L. var sativa," *Phytochemistry*, vol. 67, no. 17, pp. 1957–1963, 2006.

[15] V. Shriram, S. Jahagirdar, C. Latha et al., "A potential plasmid-curing agent, 8-epidiosbulbin E acetate, from *Dioscorea bulbifera* L. against multidrug-resistant bacteria," *International Journal of Antimicrobial Agents*, vol. 32, no. 5, pp. 405–410, 2008.

[16] T. B. Nguelefack, M. Mbiantcha, A. Kamanyi, R. B. Teponno, A. L. Tapondjou, and P. Watcho, "Analgesic and anti-inflammatory properties of extracts from the bulbils of *Dioscorea bulbifera* L. var sativa (Dioscoreaceae) in mice and rats," *Evidence-Based Complementary and Alternative Medicine*, vol. 2011, Article ID 912935, 9 pages, 2011.

[17] M. Mbiantcha, A. Kamanyi, R. B. Teponno, A. L. Tapondjou, P. Watcho, and T. B. Nguelefack, "Analgesic and anti-inflammatory properties of extracts from the bulbils of *Dioscorea bulbifera* L. var *sativa* (Dioscoreaceae) in mice and rats," *Evidence-Based Complementary and Alternative Medicine*, vol. 2011, Article ID 912935, 9 pages, 2011.

[18] Z. Ahmed, M. Z. Chishti, R. K. Johri, A. Bhagat, K. K. Gupta, and G. Ram, "Antihyperglycemic and antidyslipidemic activity of aqueous extract of *Dioscorea bulbifera* tubers," *Diabetologia Croatica*, vol. 38, no. 3, pp. 63–72, 2009.

[19] H. Gao, M. Kuroyanagi, L. Wu, N. Kawahara, T. Yasuno, and Y. Nakamura, "Antitumor-promoting constituents from *Dioscorea bulbifera* L. in JB6 mouse epidermal cells," *Biological and Pharmaceutical Bulletin*, vol. 25, no. 9, pp. 1241–1243, 2002.

[20] S. Ghosh, P. More, A. Derle et al., "Diosgenin from *Dioscorea bulbifera*: novel hit for treatment of type II diabetes mellitus with inhibitory activity against α-amylase and α-glucosidase," *PLoS ONE*, vol. 9, no. 9, Article ID e106039, 2014.

[21] S. Ghosh, M. Ahire, S. Patil et al., "Antidiabetic activity of *Gnidia glauca* and *Dioscorea bulbifera*: potent amylase and glucosidase inhibitors," *Evidence-Based Complementary and Alternative Medicine*, vol. 2012, Article ID 929051, 10 pages, 2012.

[22] S. Ghosh, A. Derle, M. Ahire et al., "Phytochemical analysis and free radical scavenging activity of medicinal plants *Gnidia glauca* and *Dioscorea bulbifera*," *PLoS ONE*, vol. 8, no. 12, Article ID e82529, 2013.

[23] S. Ghosh, S. Patil, M. Ahire et al., "Synthesis of gold nanoanisotrops using *Dioscorea bulbifera* tuber extract," *Journal of Nanomaterials*, vol. 2011, Article ID 354793, 8 pages, 2011.

[24] G. Rajamohan, V. B. Srinivasan, and W. A. Gebreyes, "Biocide-tolerant multidrug-resistant *Acinetobacter baumannii* clinical strains are associated with higher biofilm formation," *Journal of Hospital Infection*, vol. 73, no. 3, pp. 287–289, 2009.

[25] R. B. Patwardhan, P. K. Dhakephalkar, K. B. Niphadkar, and B. A. Chopade, "Incidence and prevalence of nosocomial pathogens in ICU with special reference to multiresistant *Acinetobacter baumannii* harboring multiple plasmids," *Indian Journal of Medical Research*, vol. 128, no. 8, pp. 178–187, 2008.

[26] M. R. Shakibaie, B. P. Kapadnis, P. Dhakephalker, and B. A. Chopade, "Removal of silver from photographic wastewater effluent using *Acinetobacter baumannii* BL54," *Canadian Journal of Microbiology*, vol. 45, no. 12, pp. 995–1000, 1999.

[27] P. K. Dhakephalkar and B. A. Chopade, "High levels of multiple metal resistance and its correlation to antibiotic resistance in environmental isolates of *Acinetobacter*," *BioMetals*, vol. 7, no. 1, pp. 67–74, 1994.

[28] L. M. Deshpande, B. P. Kapadnis, and B. A. Chopade, "Metal resistance in *Acinetobacter* and its relation to β-lactamase production," *Biometals*, vol. 6, no. 1, pp. 55–59, 1993.

[29] N. K. Pour, D. H. Dusane, P. K. Dhakephalkar, F. R. Zamin, S. S. Zinjarde, and B. A. Chopade, "Biofilm formation by *Acinetobacter baumannii* strains isolated from urinary tract infection and urinary catheters," *FEMS Immunology and Medical Microbiology*, vol. 62, no. 3, pp. 328–338, 2011.

[30] P. K. Sahu, P. S. Iyer, A. M. Oak, K. R. Pardesi, and B. A. Chopade, "Characterization of eDNA from the clinical strain *Acinetobacter baumannii* AIIMS 7 and its role in biofilm formation," *The Scientific World Journal*, vol. 2012, Article ID 973436, 10 pages, 2012.

[31] P. K. Sahu, P. S. Iyer, M. B. Gaikwad, S. C. Talreja, K. R. Pardesi, and B. A. Chopade, "An MFS transporter-like ORF from MDR *Acinetobacter baumannii* AIIMS 7 Is associated with adherence and biofilm formation on biotic/abiotic surface," *International Journal of Microbiology*, vol. 2012, Article ID 490647, 10 pages, 2012.

[32] D. E. Karageorgopoulos and M. E. Falagas, "Current control and treatment of multidrug-resistant *Acinetobacter baumannii* infections," *The Lancet Infectious Diseases*, vol. 8, no. 12, pp. 751–762, 2008.

[33] J. N. Palmer, "Bacterial biofilms: do they play a role in chronic sinusitis?" *Otolaryngologic Clinics of North America*, vol. 38, no. 6, pp. 1193–1201, 2005.

[34] R. L. Soon, R. L. Nation, P. G. Hartley, I. Larson, and J. Li, "Atomic force microscopy investigation of the morphology and topography of colistin-heteroresistant *Acinetobacter baumannii* strains as a function of growth phase and in response to colistin treatment," *Antimicrobial Agents and Chemotherapy*, vol. 53, no. 12, pp. 4979–4986, 2009.

[35] T. K. Berdyyeva, C. D. Woodworth, and I. Sokolov, "Human epithelial cells increase their rigidity with ageing in vitro: direct measurements," *Physics in Medicine and Biology*, vol. 50, no. 1, pp. 81–92, 2005.

[36] T. Svaldo Lanero, O. Cavalleri, S. Krol, R. Rolandi, and A. Gliozzi, "Mechanical properties of single living cells encapsulated in polyelectrolyte matrixes," *Journal of Biotechnology*, vol. 124, no. 4, pp. 723–731, 2006.

[37] I. Sokolov, "Atomic force microscopy in cancer cell research," in *Cancer Nanotechnology*, H. S. Nalwa and T. Webster, Eds., pp. 1–17, American Scientific Publishers', 2007.

[38] D. C. Lin, E. K. Dimitriadis, and F. Horkay, "Robust strategies for automated AFM force curve analysis—II: adhesion-influenced indentation of soft, elastic materials," *Journal of Biomechanical Engineering*, vol. 129, no. 6, pp. 904–912, 2007.

[39] C. C. Perry, M. Weatherly, T. Beale, and A. Randriamahefa, "Atomic force microscopy study of the antimicrobial activity of aqueous garlic versus ampicillin against *Escherichia coli* and *Staphylococcus aureus*," *Journal of the Science of Food and Agriculture*, vol. 89, no. 6, pp. 958–964, 2009.

[40] B. Shoelson, E. K. Dimitriadis, H. Cai, B. Kachar, and R. S. Chadwick, "Evidence and implications of inhomogeneity in tectorial membrane elasticity," *Biophysical Journal*, vol. 87, no. 4, pp. 2768–2777, 2004.

[41] M. Herrmann, H.-M. Lorenz, R. Voll, M. Grunke, W. Woith, and J. R. Kalden, "A rapid and simple method for the isolation of apoptotic DNA fragments," *Nucleic Acids Research*, vol. 22, no. 24, pp. 5506–5507, 1994.

[42] Y. Ma, W. Li, E. C. Cho et al., "Au@Ag core-shell nanocubes with finely tuned and well-controlled sizes, shell thicknesses, and optical properties," *ACS Nano*, vol. 4, no. 11, pp. 6725–6734, 2010.

[43] H. Liu, K. W. K. Tsim, G.-X. Chou, J.-M. Wang, L.-L. Ji, and Z.-T. Wang, "Phenolic compounds from the rhizomes of *Dioscorea bulbifera*," *Chemistry and Biodiversity*, vol. 8, no. 11, pp. 2110–2116, 2011.

[44] M. R. Bhandari and J. Kawabata, "Organic acid, phenolic content and antioxidant activity of wild yam (*Dioscorea* spp.) tubers of Nepal," *Food Chemistry*, vol. 88, no. 2, pp. 163–168, 2004.

[45] A. Narula, S. Kumar, and P. S. Srivastava, "Genetic fidelity of in vitro regenerants, encapsulation of shoot tips and high diosgenin content in *Dioscorea bulbifera* L., a potential alternative source of diosgenin," *Biotechnology Letters*, vol. 29, no. 4, pp. 623–629, 2007.

[46] G. R. Salunke, S. Ghosh, R. J. Santosh Kumar et al., "Rapid efficient synthesis and characterization of silver, gold, and bimetallic nanoparticles from the medicinal plant *Plumbago zeylanica* and their application in biofilm control," *International Journal of Nanomedicine*, vol. 9, no. 1, pp. 2635–2653, 2014.

[47] G. Park, D. Seo, J. Jung, S. Ryu, and H. Song, "Shape evolution and gram-scale synthesis of Gold@Silver core-shell nanopolyhedrons," *Journal of Physical Chemistry C*, vol. 115, no. 19, pp. 9417–9423, 2011.

[48] S. S. Shankar, A. Rai, A. Ahmad, and M. Sastry, "Rapid synthesis of Au, Ag, and bimetallic Au core-Ag shell nanoparticles using Neem (*Azadirachta indica*) leaf broth," *Journal of Colloid and Interface Science*, vol. 275, no. 2, pp. 496–502, 2004.

[49] D. S. Trentin, D. B. Silva, M. W. Amaral et al., "Tannins possessing bacteriostatic effect impair *Pseudomonas aeruginosa* adhesion and biofilm formation," *PLoS ONE*, vol. 8, no. 6, Article ID e66257, 2013.

[50] K.-H. Cho, J.-E. Park, T. Osaka, and S.-G. Park, "The study of antimicrobial activity and preservative effects of nanosilver ingredient," *Electrochimica Acta*, vol. 51, no. 5, pp. 956–960, 2005.

[51] N. R. Panyala, E. M. Peña-Méndez, and J. Havel, "Silver or silver nanoparticles: a hazardous threat to the environment and human health?" *Journal of Applied Biomedicine*, vol. 6, no. 3, pp. 117–129, 2008.

[52] P. E. Fournier and H. Richet, "The epidemiology and control of *Acinetobacter baumannii* in health care facilities," *Clinical Infectious Diseases*, vol. 42, no. 5, pp. 692–699, 2006.

[53] A. Jawad, J. Heritage, A. M. Snelling, D. M. Gascoyne-Binzi, and P. M. Hawkey, "Influence of relative humidity and suspending

menstrua on survival of *Acinetobacter* spp. on dry surfaces," *Journal of Clinical Microbiology*, vol. 34, no. 12, pp. 2881–2887, 1996.

[54] M. R. Shakibaie, P. K. Dhakephalker, B. P. Kapadnis, G. A. Salajaghe, and B. A. Chopade, "Plasmid mediated silver and antibiotic resistance in *Acinetobacter baumannii* BL54," *Iranian Journal of Medical Sciences*, vol. 23, no. 1-2, pp. 30–36, 1998.

[55] L. M. Deshpande and B. A. Chopade, "Plasmid mediated silver resistance in *Acinetobacter baumannii*," *BioMetals*, vol. 7, no. 1, pp. 49–56, 1994.

[56] E. G. Playford, J. C. Craig, and J. R. Iredell, "Carbapenem-resistant *Acinetobacter baumannii* in intensive care unit patients: risk factors for acquisition, infection and their consequences," *The Journal of Hospital Infection*, vol. 65, no. 3, pp. 204–211, 2007.

[57] C. Carlson, S. M. Hussein, A. M. Schrand et al., "Unique cellular interaction of silver nanoparticles: size-dependent generation of reactive oxygen species," *The Journal of Physical Chemistry B*, vol. 112, no. 43, pp. 13608–13619, 2008.

[58] N. K. Palanisamy, N. Ferina, A. N. Amirulhusni et al., "Antibiofilm properties of chemically synthesized silver nanoparticles found against *Pseudomonas aeruginosa*," *Journal of Nanobiotechnology*, vol. 12, no. 1, article 2, 2014.

[59] S. Chatterjee, A. Bandyopadhyay, and K. Sarkar, "Effect of iron oxide and gold nanoparticles on bacterial growth leading towards biological application," *Journal of Nanobiotechnology*, vol. 9, article 34, 2011.

[60] W. Ghandour, J. A. Hubbard, J. Deistung, M. N. Hughes, and R. K. Poole, "The uptake of silver ions by *Escherichia coli* K12: toxic effects and interaction with copper ions," *Applied Microbiology and Biotechnology*, vol. 28, no. 6, pp. 559–565, 1988.

[61] H. G. Petering, "Pharmacology and toxicology of heavy metals: silver," *Pharmacology and Therapeutics Part A : Chemotherapy, Toxicology and Metabolic Inhibitors*, vol. 1, no. 2, pp. 127–130, 1976.

[62] W. J. A. Schreurs and H. Rosenberg, "Effect of silver ions on transport and retention of phosphate by *Escherichia coli*," *Journal of Bacteriology*, vol. 152, no. 1, pp. 7–13, 1982.

[63] P. D. Bragg and D. J. Rainnie, "The effect of silver ions on the respiratory chain of *Escherichia coli*," *Canadian Journal of Microbiology*, vol. 20, no. 6, pp. 883–889, 1974.

[64] A. M. Allahverdiyev, E. S. Abamor, M. Bagirova et al., "Antileishmanial effect of silver nanoparticles and their enhanced antiparasitic activity under ultraviolet light," *International journal of Nanomedicine*, vol. 6, pp. 2705–2714, 2011.